Electron Accumulation and Emergent Magnetism in LaMnO_{3}/SrTiO_{3} Heterostructures

Zuhuang Chen, Zhanghui Chen, Z. Q. Liu, M. E. Holtz, C. J. Li, X. Renshaw Wang, W. M. Lü, M. Motapothula, L. S. Fan, J. A. Turcaud, L. R. Dedon, C. Frederick, R. J. Xu, R. Gao, A. T. N'Diaye, E. Arenholz, J. A. Mundy, T. Venkatesan, D. A. Muller, L.-W. Wang, Jian Liu, and L. W. Martin

Phys. Rev. Lett. **119**, 156801 — Published 11 October 2017

DOI: 10.1103/PhysRevLett.119.156801

Electron Accumulation and Emergent Magnetism in $LaMnO_3/SrTiO_3$ Heterostructures

Zuhuang Chen[1,2], Zhanghui Chen[2], Z. Q. Liu[3*], M. E. Holtz[4], C. J. Li[5,6], X. Renshaw Wang[7], W. M. Lü[8], M. Motapothula[6], L. S. Fan[9], J. A. Turcaud,[1] L. R. Dedon[1], C. Frederick[10], R. J. Xu,[1] R. Gao,[1] A. T. N'Diaye[11], E. Arenholz[11], J. A. Mundy[1,2], T. Venkatesan[5,6], D. A. Muller[4], L.-W. Wang[2], J. Liu[10*], and L. W. Martin[1,2*]

[1] Department of Materials Science and Engineering, University of California, Berkeley, California 94720, USA

[2] Materials Science Division, Lawrence Berkeley National Laboratory, Berkeley, California 94720, USA

[3] School of Materials Science and Engineering, Beihang University, Beijing 100191, China

[4] School of Applied and Engineering Physics, Cornell University, Ithaca, New York 14853, USA

[5] Department of Materials Science and Engineering, National University of Singapore, Singapore 117575, Singapore

[6] NUSNNI-Nanocore, National University of Singapore, Singapore 117411, Singapore

[7] School of Physical and Mathematical Sciences & School of Electrical and Electronic Engineering, Nanyang Technological University, Singapore 637371

[8] Condensed Matter Science and Technology Institute, School of Science, Harbin Institute of Technology, Harbin 150081, People's Republic of China

[9] Center for Nanophase Materials Sciences, Oak Ridge National Laboratory, Oak Ridge, Tennessee 37831, USA

[10] Department of Physics and Astronomy, University of Tennessee, Knoxville, Tennessee 37996, USA

[11] Advanced Light Source, Lawrence Berkeley National Laboratory, Berkeley, California 94720, USA

*Email: zhiqi@buaa.edu.cn; jianliu@utk.edu; lwmartin@berkeley.edu

Abstract:

Emergent phenomena at polar-nonpolar oxide interfaces have been studied intensely in pursuit of next-generation oxide electronics and spintronics. Here we report the disentanglement of critical thicknesses for electron reconstruction and the emergence of ferromagnetism in polar-mismatched $LaMnO_3/SrTiO_3$ (001) heterostructures. Using a combination of element-specific X-ray absorption spectroscopy and dichroism, and first-principles calculations, interfacial electron accumulation and ferromagnetism have been observed *within* the polar, antiferromagnetic insulator $LaMnO_3$. Our results show that the critical thickness for the onset of electron accumulation is as thin as 2 unit cells (UC), significantly thinner than the observed critical thickness for ferromagnetism of 5 UC. The absence of ferromagnetism below 5 UC is likely induced by electron over-accumulation. In turn, by controlling the doping of the $LaMnO_3$, we are able to neutralize the excessive electrons from the polar mismatch in ultrathin $LaMnO_3$ films and thus enable ferromagnetism in films as thin as 3 UC, extending the limits of our ability to synthesize and tailor emergent phenomena at interfaces and demonstrating manipulation of the electronic and magnetic structures of materials at the shortest length scales.

The observation of emergent interfacial electronic reconstruction and, in turn, new electronic phases at polar/non-polar oxide interfaces have launched numerous studies on the fundamental mechanisms for and potential uses of these exotic properties [1-3]. The nature of such electronic reconstruction (used here in the broad sense as any change in valence that results from the interfacial polar mismatch) depends on many factors such as the interfacial band alignment and the conductivity of the materials that can alter the boundary conditions and thus the degree of charge compensation [4]. To date, the most widely-studied system in this regard is the two-dimensional electron gas in $LaAlO_3/SrTiO_3$ [5]. $LaAlO_3$ is an insulator with a band gap of 5.6 eV which consists of alternating charged $(LaO)^+$ and $(AlO_2)^-$ layers along the [001]. $SrTiO_3$ is also an insulator, with a band gap of 3.2 eV, which has neutral $(SrO)^0$ and $(TiO_2)^0$ layers alternating along the [001]. When these materials are brought together, a so-called *polarization catastrophe* is believed to occur at the (001) interface due to a potential build-up in the polar $LaAlO_3$ which drives charge transfer from the $LaAlO_3$ valence band to the $SrTiO_3$ conduction band at a $LaAlO_3$ critical thickness of 4 unit cells (UC) [6-8]. As a result, there is electron-doping into the $SrTiO_3$ near the interface, which induces a reduction of Ti^{4+} towards Ti^{3+} [9] and the onset of conductivity [2]. Meanwhile, there have been reports of other exotic interfacial phenomena, such as orbital reconstruction [10], ferromagnetism [11], and superconductivity [12], and researchers have also explored the role that structural imperfections can play in the evolution of effects at these interfaces [13-17].

Since the initial observation of emergent phenomena at the $LaAlO_3/SrTiO_3$ heterointerface, a number of additional systems have been found to exhibit similar potential build-up induced electronic reconstruction and interfacial phenomena (*e.g.*, $LaTiO_3/SrTiO_3$ [18], $LaVO_3/SrTiO_3$ [19], $NdTiO_3/SrTiO_3$ [20], etc.). Studies of other related polar/non-polar

interfaces, namely $LaCrO_3/SrTiO_3$ [21] and $LaMnO_3/SrTiO_3$ [22], however, have suggested that this rule is not universal since no critical-thickness for a metal-to-insulator transition was found in either system. At first glance this is surprising since, for example, $LaMnO_3$ is constructed from alternating $(LaO)^+$ and $(MnO_2)^-$ layers and thus electronic reconstruction akin to that in $LaAlO_3/SrTiO_3$ should be expected. Initially, the lack of metallic conductivity was enough to discourage researchers from further study, but it does not necessarily mean that the interfacial polar mismatch does not have some influence on the charge or spin degrees of freedom. In fact, recent work on the $LaMnO_3/SrTiO_3$ system has proposed that charge transfer may occur within $LaMnO_3$ as a result of a similar potential build-up which produces electron doping near the interface and hole doping near the surface and subsequently gives rise to ferromagnetism in $LaMnO_3$ [23, 24]. Direct evidence for the electron reconstruction and the nature of magnetism has not, however, been reported, precluding further understanding and control of the functional properties.

In this work, we apply X-ray absorption spectroscopy (XAS) and magnetic circular dichroism (XMCD), and first-principles calculations to investigate the effect of polar mismatch on the electronic and magnetic structure of the polar, antiferromagnetic insulator $LaMnO_3$ grown on nonpolar $SrTiO_3$. XAS reveals a significant change of the Mn valence state in $LaMnO_3$ even in 2- UC-thick films, but no change in Ti valence in the $SrTiO_3$. XMCD, on the other hand, reveals ferromagnetism with a critical thickness of 5 UC. The decoupling of the charge and magnetic critical thicknesses and the absence of hole doping near the film surface suggest that the charge transfer picture [23, 24] may not be directly applicable or is an oversimplification. Theoretical studies show that the potential build-up in the $LaMnO_3$ is 0.177 V/Å and this, together with the small band gap of $LaMnO_3$, results in a critical thickness for the built-in

potential to collapse at only 2 UC. In turn, we identify a chemical route – whereby small changes in film stoichiometry – can be used to effectively control the doping level and modulate the influence of the polar mismatch so as to induce ferromagnetism in films down to just 3 UC.

$LaMnO_3$ films were grown on TiO_2-terminated $SrTiO_3$ (001) substrates by reflection high-energy electron diffraction (RHEED)-assisted pulsed-laser deposition [25]. For all films, RHEED intensity oscillations were persistent throughout the growth indicating a layer-by-layer growth mode [25]. Further characterization of the heterostructures reveal high-quality $LaMnO_3$ films with atomically-smooth surfaces and high crystalline quality, and interfaces that are free of dislocations [25]. To probe the potential for electron reconstruction and associated ferromagnetic order, we have performed soft XAS and XMCD studies in a grazing incidence, total electron yield (TEY) geometry on numerous $LaMnO_3/SrTiO_3$ heterostructures (inset, Fig. 1a) [25]. Compared to previous local magnetometry studies using a scanning superconducting quantum interference device (SQUID) [23, 24], the current approach is surface sensitive and provides a direct measurement of the valence state of the various elements in the films and substrates *via* XAS and enables the detection of subtle (~ 0.005 μ_B/atom), element-specific magnetic moments (thus excluding magnetic impurities) *via* XMCD [9]. XMCD measurements at the Mn $L_{2,3}$ edges at 25 K reveal strong dichroism (Fig. 1a), indicative of a net ferromagnetic moment, arising from Mn in the films. XMCD of ~28% and ~26% is observed for the 9 and 12 UC thick $LaMnO_3$ films, respectively. To give this some context, the corresponding SQUID magnetometry measurement on the 9 UC thick $LaMnO_3/SrTiO_3$ heterostructure revealed a magnetic moment of ~400 emu/cc at 25 K [25]. The XMCD is reduced to ~22% for the 6 UC films and finally to ~11% for the 5 UC films. There are a number of important observations to be noted here. First, due to the high sensitivity of the XMCD, we are able to detect the small magnetic moment of the 5 UC thick

films, something not accomplished in previous studies [23]. Second, the large XMCD in the $LaMnO_3$ films as thin as 9 UC is comparable to that observed in hole-doped $La_{0.67}Sr_{0.33}MnO_3$ [40].

These thickness-dependent XMCD results confirm the existence of intrinsic magnetization in the $LaMnO_3$ films, in line with previous magnetometry studies [23, 24]. To understand the nature of the magnetism, we first performed XAS measurements at both the Ti- and Mn-$L_{2,3}$ edges as a function of $LaMnO_3$ thickness to probe the corresponding evolution of the valence states. Regardless of the $LaMnO_3$ thickness, the Ti-$L_{2,3}$ edges are unchanged and match that of a $SrTiO_3$ substrate reference (Fig. 1b). In other words, there is no indication of electron transfer to the $SrTiO_3$ and the bulk-like character of Ti^{4+} is maintained at the $LaMnO_3/SrTiO_3$ heterointerface. In contrast, XAS studies at the Mn-$L_{2,3}$ edges reveal marked variation with film thickness (Fig. 1c). To understand the evolution of the Mn valence state, we provide spectra for bulk $SrMnO_3$ (*i.e.*, Mn^{4+} reference), $LaMnO_3$ (*i.e.*, Mn^{3+} reference), and MnO (*i.e.*, Mn^{2+} reference) for comparison [41, 42]. Starting with relatively thick $LaMnO_3$ films (*e.g.*, 12 UC), the absorption spectra are observed to be similar to that of bulk $LaMnO_3$, indicating a predominant Mn^{3+} valence state. Note that the absorption peak has a slightly lower energy position than that of bulk $LaMnO_3$, indicating that the films are somewhat electron doped. Upon reducing the $LaMnO_3$ thickness (*e.g.*, 9 UC) a shift of the main spectral feature near 641.4 eV to lower energies is observed, indicating a lower average valence state. Further reducing the $LaMnO_3$ thickness (*e.g.*, 6, 5, and 3 UC) results in further shifts of the feature. Moreover, a strong feature near 640 eV appears which corresponds to the main absorption peak of Mn^{2+}. Note that the suppression of the fine feature at ~638 eV in our ultrathin $LaMnO_3$ films, as compared to the MnO reference spectrum, is likely due to different local environments for the two structures

[43]. Similar studies of 2 UC thick heterostructures likewise reveal a strong feature from Mn^{2+} [25]; these data are not shown on the same graph since sample charging distorts the background of the spectra. Our XAS studies clearly show that the average Mn valence state within the thin samples is reduced, and further suggest that electrons are accumulated in the $LaMnO_3$ layer near the interface starting at a critical thickness of 2 UC. This is in contrast to our above XMCD studies and the previous local magnetometry studies [23, 24], which found that the emergent ferromagnetism is not measureable until a thickness 5-6 UC. That is, there is a decoupling of the electron accumulation and ferromagnetic critical thicknesses.

Furthermore, our studies are completed in TEY geometry which probes the topmost 3-5 nm of thin-film samples such that the contribution of the deeper layers to the TEY intensity decays exponentially with the distance from the film surface. Therefore, with increasing $LaMnO_3$ layer thickness the contribution of the Mn at the interface decreases accordingly. The observed decrease of Mn^{2+} signatures in the Mn XAS spectra with increasing $LaMnO_3$ layer thickness suggests that the valence state is likely non-uniform along the surface normal. Thus, we find that the fraction of Mn^{2+} is higher in the thinner films where the interface contributes more to the Mn XAS signal. This variation in valence state with film thickness is also evident in the evolution of the O *K* edge [25]. It is possible that the bottom 3 UC, near the interfacial region, remains Mn^{2+}-rich for the 5 and 6 UC samples [44]. As the thickness increases beyond 6 UC, the thickness becomes comparable or larger than the probing depth and the contribution from the interfacial region to the spectrum is reduced. To compensate for the polar field, the excess electrons are likely to accumulate at the interface, creating an inhomogeneous charge profile across the film thickness. Such an observation is consistent with studies of $La_{1-x}Sr_xMnO_3/SrTiO_3$ (001) heterostructures wherein excess electrons are found to reside near the interfaces [44].

The presence of this electron accumulation due to the polar mismatch is further supported by similar XAS studies of $LaMnO_3/NdGaO_3$ $(110)_O$ heterostructures (subscript O denotes orthorhombic index). The $NdGaO_3$ substrates were treated to produce GaO_2-terminated surfaces which are polar in nature [45], consequently, there should be *no* polar mismatch at the $LaMnO_3/NdGaO_3$ heterointerface. XAS spectra at the Mn-$L_{2,3}$ edges are characteristic of bulk-like Mn^{3+} with no Mn^{2+} features (even for 3 UC thick films), and there is no thickness dependence of the XAS spectra (Fig. 1d); thus no excess charge is observed in the $LaMnO_3/NdGaO_3$ heterostructures. Ultimately, these studies indicate that electrons accumulate in the $LaMnO_3$ near the interfaces to alleviate the *polar catastrophe* in the $LaMnO_3/SrTiO_3$ heterostructures at film thicknesses as small as 2 UC.

To understand the origin of the electron accumulation, the band offset at the $LaMnO_3/SrTiO_3$ interface and the potential build-up in the $LaMnO_3$ were computed for symmetric $(LaMnO_3)_m/(SrTiO_3)_n/(LaMnO_3)_m$ (n = 4.5, m = 2, 4, 6 UC) structures (Fig. 2a, m = 4 UC) using first-principles density functional theory (DFT) [25]. The resulting in-plane-averaged (oscillating blue line) and macroscopically-averaged (red line) electrostatic potentials reveal a potential build-up in the $LaMnO_3$ layers due to the alternating charged atomic layers along the surface normal (Fig. 2b, m = 4). An average slope for the potential evolution was extracted for heterostructures with m = 2, 4 (Fig. 2c) from which the average internal field is determined to be ~0.177 V/Å. This internal field is smaller than that reported for the $LaAlO_3/SrTiO_3$ system (0.24 V/Å) [7] and the difference could be due to the different screening effects of $LaAlO_3$ and $LaMnO_3$. The calculated potential build-up is based on an idealized abrupt interface without defects and adsorbates. Such a potential build-up, however, has been difficult to detect experimentally (see Figs. 35-37, Ref. [15]) and is still under debate. Additionally, by evaluating

the average potential in bulk and multi-layer heterostructures, the valence band offset between the $LaMnO_3$ and $SrTiO_3$ was extracted to be ~0.6 eV [25]. This, combined with the large difference in band gap between $LaMnO_3$ (1.3 eV) and $SrTiO_3$ (3.2 eV) [25], results in a straddling band configuration at the $LaMnO_3/SrTiO_3$ interface (Fig. 2d). Based on these two facts, electron accumulation is expected to occur when the built-in potential in the $LaMnO_3$ layer surpasses the $LaMnO_3$ band gap, which is calculated to happen at a critical thickness of ~7.3 Å (just less than 2 UC of $LaMnO_3$). As a result, the system will become unstable and must find a way to compensate the potential. Because the potential difference is positive from the interface to the surface, the screening or compensation effect will always tend to accumulate negative charges near the interface. This naturally explains the reduction of the Mn^{3+} towards Mn^{2+} in the very thin limit and near the interfaces for thicker samples. This is different from the case of $LaAlO_3/SrTiO_3$, where the $LaAlO_3$ band gap straddles the $SrTiO_3$ bands, thus the negative charges stay in the $SrTiO_3$ near the interface and reduce the Ti^{4+} towards Ti^{3+} [7-9].

Intriguingly, no indication of Mn^{4+} was detected at/near the $LaMnO_3$ film surfaces, implying that the previous proposed charge transfer model [23, 24] could be oversimplified or may not be directly applicable to this system. In turn, any number of additional surface structural or chemical reconstructions could possibly occur to adequately compensate for the electron accumulation [46-49]. Furthermore, oxygen vacancies, in particular, have been considered as a means to compensate the polar field [48-50]. In these $LaMnO_3/SrTiO_3$ heterostructures, there is no evidence for the reduction of and oxygen vacancy formation in the $SrTiO_3$ since there was no signature of Ti^{3+} detected via XAS near the interface and the heterostructures show insulating behavior [25]. Furthermore, there is no evidence for a large concentration of oxygen vacancies in either the film or substrate as a result of the growth process. This is supported by the lack of

evidence for Mn^{2+} in $LaMnO_3/NdGaO_3$ heterostructures which, despite being fabricated at the same conditions, show no evidence of a change in the valence state. Both of these observations are consistent with the high oxygen growth pressure (10^{-2} mbar) [25]. In turn, the emergence of Mn^{2+} in the $LaMnO_3/SrTiO_3$ heterostructures is attributed to the polar discontinuity at the heterointerface regardless of the specific mechanism responsible for the electron accumulation which could be electronic, structural, and/or chemical in nature [46-51]. Oxygen vacancies (not necessarily induced by deposition) have been proposed to be an intrinsic compensation mechanism for polar/nonpolar oxide heterostructures, which would lead to electron accumulation at the interface [48, 49, 51].

Bulk, stoichiometric $LaMnO_3$ with Mn^{3+} is an *A*-type antiferromagnetic insulator [52]. Despite a possible electron-hole asymmetry in the manganite phase diagram similar to cuprates [53], the addition of either extra holes or electrons via chemical doping could lead to ferromagnetism as a result of Mn^{3+}-O^{2-}-Mn^{4+} or Mn^{3+}-O^{2-}-Mn^{2+} double exchange, respectively [52, 54-57]. It is known that extrinsic defects, such as cation-deficiency (*e.g.*, La-deficiency) or oxygen-excess, could give rise to ferromagnetism in $LaMnO_3$ [58, 59]. However, $LaMnO_3$ with cation deficiency or oxygen-excess tends to be a ferromagnetic metal with a mixture of Mn^{3+} and Mn^{4+} (*i.e.*, hole doping) [60], which is not consistent with the observation that our films are electron doped with nominal cation stoichiometry and insulating behavior [25]. Therefore, in our work, the emergence of electron doping at the $LaMnO_3/SrTiO_3$ interface triggered by the polar mismatch induces a mixed valence (*i.e.*, Mn^{2+}/Mn^{3+}) which is thought to give rise to the ferromagnetic phase [52, 54-57]. In fact, both the XAS and XMCD spectra observed in our relatively thick $LaMnO_3/SrTiO_3$ heterostructures (Fig. 1a,c) are similar to that of electron-doped

manganites deriving their effects from chemical alloying (*e.g.*, Ce-doped $LaMnO_3$), which also exhibit an insulating ferromagnetic ground state [57].

The absence of ferromagnetism for films less than 5 UC is likely due to "over accumulation" of Mn^{2+} (stemming from the need to localize a significant number of electrons to accommodate the potential and resulting in reduced magnetization from a lack of double-exchange coupling with Mn^{3+}) which favors an antiferromagnetic state [55]. In turn, we explored the possibility of reducing the Mn^{2+} component by adjusting the composition of the films to confirm our understanding of the origin of the ferromagnetism and demonstrating the potential of such systems. Previous studies have found that La-vacancies give rise to hole doping in $LaMnO_3$ [58, 60]. Thus, we have grown 5% La-deficient $LaMnO_3$ ($La_{0.95}MnO_3$) films of varying thicknesses on $SrTiO_3$ substrates [25] to induce holes which should act to counter-dope the system under the influence of the potential and thus reduce the amount of Mn^{2+} in the ultra-thin films (*i.e.*, drive it back from an over-electron-doped state to a more "optimally-doped" level). La-deficiency is an effective route to introduce holes into $LaMnO_3$ via the defect formula $(\mathrm{La}^{3+}_{1-x}[V_{La}^{3-}]_x)(Mn^{3+}_{1-3x}Mn^{4+}_{3x})O_3^{2-}$. The $La_{0.95}MnO_3$ exhibits alternating $(La_{1-x}O)^{1-3x}$ and $(Mn^{3+}_{1-3x}Mn^{4+}_{3x}O_2)^{-1+3x}$ layers and thus a polar mismatch still exists at the $La_{0.95}MnO_3/SrTiO_3$ interface. Due to the La-deficiency, the magnitude of the polar discontinuity would be reduced with additional holes. From XAS studies of these $La_{0.95}MnO_3$ films, a weaker thickness dependence of the Mn valence is observed (Fig. 3a). In particular, the peak corresponding to Mn^{2+} at 639.8 eV is suppressed in the 3 UC thick $La_{0.95}MnO_3$ films. In turn, subsequent XMCD studies reveal clear dichroism even in 3 UC thick $La_{0.95}MnO_3/SrTiO_3$ heterostructures (Fig. 3b) – confirming the importance of controlling the valence state of the material to relieve the over accumulation of electrons. All told, the observation of an insulating ferromagnetic ground state

in films as thin as just 3 UC shows the power of emergent phenomena and approaches the limits of our ability to synthesize and study emergent phenomena at interfaces, and has potential applications in spin polarized tunneling devices.

To summarize, we have provided direct evidence for electron accumulation and ferromagnetism occurring within the polar, antiferromagnetic insulator $LaMnO_3$ when grown on non-polar $SrTiO_3$. Using XAS combined with first-principles calculations, the critical thickness for the onset of electron accumulation is determined to be 2 UC. The strength of the polar mismatch can drive "over-doping" of the $LaMnO_3$ which suppresses the onset of ferromagnetism as the average valence state tips towards Mn^{2+}. In stoichiometric $LaMnO_3$, ferromagnetism is observed in only 5 UC thick films. In turn, through chemical doping (achieved via control of the film stoichiometry), the average valence state can be tuned, and clear ferromagnetism can be observed in $La_{0.95}MnO_3$ films as thin as 3 UC. Ultimately, this work demonstrates the state-of-the-art as it pertains to ultra-fine control of materials, whereby controlling both the atomic-structure of interfaces and doping level, unprecedented properties and control of materials is produced.

Acknowledgement

Z.H.C. would like to thank Dr. Chang-Yang Kuo for useful discussion and acknowledge support from the Laboratory Directed Research and Development Program of Lawrence Berkeley National Laboratory under U.S. Department of Energy Contract No. DE-AC02-05CH11231. Z.C. and L.-W.W. acknowledges the support from the U.S. Department of Energy, Office of Science, Office of Basic Energy Sciences, Materials Sciences and Engineering Division, of the under Contract No. DE-AC02-05-CH11231 within the Non-Equilibrium Magnetic Materials program (MSMAG). Z.Q.L. acknowledges financial support of the startup grant from Beihang University, China. X.R.W. acknowledges supports from startup grant from Nanyang Technological University. L.R.D. acknowledges support from the Department of Energy under Grant No. DE-SC0012375. R.X. acknowledges support from the National Science Foundation under grant DMR-1608938. R.G. acknowledges support from the National Science Foundation under grant OISE-1545907. T.V. acknowledges support from the Singapore National Research Foundation (NRF) Competitive Research Program (CRP Award No. NFR-CRP13-2014-04). J.L. acknowledges support from the Science Alliance Joint Directed Research and Development Program at the University of Tennessee. L.W.M. acknowledges supports from the Gordon and Betty Moore Foundation's EPiQS Initiative, Grant GBMF5307. Work performed at the electron microscopy facility of the Cornell Center for Materials Research was funded by the National Science Foundation (NSF) Materials Research Science and Engineering Centers program (DMR 1120296) and U.S. Department of Energy, Office of Basic Energy Sciences, Division of Materials Sciences and Engineering, under Award No. DE-SC0002334. The Advanced Light Source is supported by the Director, Office of Science, Office of Basic Energy Sciences, of the US DOE under Contract DE-AC02-05CH11231.

References

[1] A. Ohtomo, D.A. Muller, J. L. Grazul, H. Y. Hwang, Nature **419**, 378 (2002).

[2] A. Ohtomo, H. Y. Hwang, Nature, **427**, 423 (2004).

[3] H. Y. Hwang, Y. Iwasa, M. Kawasaki, B. Keimer, N. Nagaosa, Y. Tokura, Nat. Mater., **11**, 103 (2012).

[4] H. Seungbum, M. N. Serge, & D. F. Dillon, Rep. Prog. Phys. **79**, 076501 (2016).

[5] J. Mannhart, D. G. Schlom, Science, **327**, 1607 (2010).

[6] S. Thiel, G. Hammerl, A. Schmehl, C. W. Schneider, J. Mannhart, Science, **313**, 1942, (2006).

[7] J. Lee, A. A. Demkov, Phys. Rev. B **78**, 193104 (2008).

[8] J. W. Park, D. F. Bogorin, C. Cen, D. A. Felker, Y. Zhang, C. T. Nelson, C. W. Bark, C. M. Folkman, X. Q. Pan, M. S. Rzchowski, J. Levy, C. B. Eom, Nat. Commun., **1**, 94 (2010).

[9] J. S. Lee, Y. W. Xie, H. K. Sato, C. Bell, Y. Hikita, H. Y. Hwang, C.C. Kao, Nat. Mater., **12**, 703-706 (2013).

[10] M. Salluzzo, J. C. Cezar, N. B. Brookes, V. Bisogni, G. M. De Luca, C. Richter, S. Thiel, J. Mannhart, M. Huijben, A. Brinkman, G. Rijnders, G. Ghiringhelli, Phys. Rev. Lett. **102**, 166804 (2009).

[11] A. Brinkman, M. Huijben, M. van Zalk, J. Huijben, U. Zeitler, J. C. Maan, W. G. van der Wiel, G. Rijnders, D. H. A. Blank, H. Hilgenkamp, Nat. Mater., **6**, 493 (2007).

[12] N. Reyren, S. Thiel, A. D. Caviglia, L. F. Kourkoutis, G. Hammerl, C. Richter, C. W. Schneider, T. Kopp, A. S. Ruetschi, D. Jaccard, M. Gabay, D. A. Muller, J. M. Triscone, J. Mannhart, Science, **317**, 1196 (2007).

[13] W. Siemons, G. Koster, H. Yamamoto, W. A. Harrison, G. Lucovsky, T. H. Geballe, D. H. A. Blank, M.R. Beasley, Phys. Rev. Lett. **98**, 196802 (2007).

[14] G. Herranz, M. Basletić, M. Bibes, C. Carrétéro, E. Tafra, E. Jacquet, K. Bouzehouane, C. Deranlot, A. Hamzić, J. M. Broto, A. Barthélémy, A. Fert, Phys. Rev. Lett. **98**, 216803 (2007).

[15] S. A. Chambers, M. H. Engelhard, V. Shutthanandan, Z. Zhu, T. C. Droubay, L. Qiao, P. V. Sushko, T. Feng, H. D. Lee, T. Gustafsson, E. Garfunkel, A. B. Shah, J. M. Zuo, Q. M. Ramasse, Surf. Sci. Rep. **65**, 317 (2010).

[16] E. Breckenfeld, N. Bronn, J. Karthik, A. R. Damodaran, S. Lee, N. Mason, L. W. Martin, Phys. Rev. Lett. **110**, 196804 (2013).

[17] Z.□Q. Liu, C.□J. Li, W.□M. Lü, X.□H. Huang, Z. Huang, S.□W. Zeng, X.□P. Qiu, L.□S. Huang, A. Annadi, J.□S. Chen, J.□M.□D. Coey, T. Venkatesan, and Ariando, Phys. Rev. X **3**, 021010 (2013).

[18] J. S. Kim, S. S. A. Seo, M. F. Chisholm, R. K. Kremer, H. U. Habermeier, B. Keimer, H.N. Lee, Phys. Rev. B **82**, 201407 (2010).

[19] Y. Hotta, T. Susaki, H. Y. Hwang, Phys. Rev. Lett. **99**, 236805 (2007).

[20] P. Xu, Y. Ayino, C. Cheng, V.S. Pribiag, R.B. Comes, P.V. Sushko, S.A. Chambers, B. Jalan, Phys. Rev. Lett. **117**, 106803(2016).

[21] S.A. Chambers, L. Qiao, T.C. Droubay, T.C. Kaspar, B. W. Arey, P. V. Sushko, Phys. Rev. Lett. **107**, 206802 (2011).

[22] P. Perna, D. Maccariello, M. Radovic, U. Scotti di Uccio, I. Pallecchi, M. Codda, D. Marré, C. Cantoni, J. Gazquez, M. Varela, S. J. Pennycook, F. M. Granozio, Appl. Phys. Lett. **97**, 152111 (2010).

[23] X. R. Wang, C. J. Li, W. M. Lü, T. R. Paudel, D. P. Leusink, M. Hoek, N. Poccia, A. Vailionis, T. Venkatesan, J. M. D. Coey, E. Y. Tsymbal, Ariando, H. Hilgenkamp, Science **349**, 716 (2015).

[24] Y. Anahory, L. Embon, C. J. Li, S. Banerjee, A. Meltzer, H. R. Naren, A. Yakovenko, J. Cuppens, Y. Myasoedov, M. L. Rappaport, M. E. Huber, K. Michaeli, T. Venkatesan, Ariando, E. Zeldov, Nat. Commun., **7**, 12566 (2016).

[25] See supplementary material at http://link.aps.org/supplemental/ for details on films growth, structural characterization, soft X-ray absorption measurement, transport and magnetic properties characterizations, and first-principles calculations which includes Refs. [26-39].

[26] L. F. Kourkoutis, J. H. Song, H. Y. Hwang, D. A. Muller, Proc. Natl. Acad. Sci. U.S.A. 107, 11682 (2010).

[27] A. Tebano, C. Aruta, S. Sanna, P.G. Medaglia, G. Balestrino, A.A. Sidorenko, R. De Renzi, G. Ghiringhelli, L. Braicovich, V. Bisogni, N.B. Brookes, Phys. Rev. Lett. 100, 137401 (2008).

[28] D. Pesquera, G. Herranz, A. Barla, E. Pellegrin, F. Bondino, E. Magnano, F. Sánchez, J. Fontcuberta, Nat Commun, 3, 1189 (2012).

[29] D.-Y. Cho, S.J. Oh, D.G. Kim, A. Tanaka, J.H. Park, Phys. Rev. B 79, 035116 (2009).

[30] M. Abbate, F.M.F. de Groot, J.C. Fuggle, A. Fujimori, O. Strebel, F. Lopez, M. Domke, G. Kaindl, G.A. Sawatzky, M. Takano, Y. Takeda, H. Eisaki, S. Uchida, Phys. Rev. B 46, 4511 (1992).

[31] G. Subias, J. García, M. C. Sánchez, J. Blasco, and M. G. Proietti, Surf. Rev. Lett. 09, 1071 (2002).

[32] P.E. Blöchl, Phys. Rev. B 50, 17953-17979 (1994).

[33] G. Kresse, D. Joubert, Phys. Rev. B 59, 1758-1775 (1999).

[34] G. Kresse, J. Hafner, Phys. Rev. B 47, 558-561 (1993).

[35] G. Kresse, J. Furthmüller, Phys. Rev. B 54, 11169-11186 (1996).

[36] J.P. Perdew, K. Burke, M. Ernzerhof, Phys. Rev. Lett. 77, 3865-3868 (1996).

[37] H.J. Monkhorst, J.D. Pack, Phys. Rev. B 13, 5188-5192 (1976).

[38] Y. Li, & J. Yu, *J. Appl. Phys.* **108**, 013701 (2010).

[39] G. Singh-Bhalla, C. Bell, J. Ravichandran, W. Siemons, Y. Hikita, S. Salahuddin, A.□F. Hebard, H.□Y. Hwang, and R. Ramesh, *Nat Phys* **7**, 80-86, (2011).

[40] F. Yang, M. Gu, E. Arenholz, N. D. Browning, Y. Takamura, J. Appl. Phys. **111**, 013911 (2012).

[41] C. Mitra, Z. Hu, P. Raychaudhuri, S. Wirth, S.I. Csiszar, H.H. Hsieh, H.J. Lin, C.T. Chen, L.H. Tjeng, Phys. Rev. B **67**, 092404 (2003).

[42] T. Burnus, Z. Hu, H. H. Hsieh, V. L. J. Joly, P. A. Joy, M. W. Haverkort, H. Wu, A. Tanaka, H.-J. Lin, C. T. Chen, and L. H. Tjeng, Phys. Rev. B 77, 125124 (2008).

[43] M. Nagel, I. Biswas, P. Nagel, E. Pellegrin, S. Schuppler, H. Peisert, and T. Chasse, Phys.Rev. B 75, 195426 (2007).

[44] J. A. Mundy, Y. Hikita, T. Hidaka, T. Yajima, T. Higuchi, H. Y. Hwang, D. A. Muller, L. F. Kourkoutis, Nat Commun, **5**, 3464 (2014).

[45] V. Leca, D. H. A. Blank, and G. Rijnders, arXiv:1202.2256 (2012).

[46] R. Pentcheva and W.□E. Pickett, Phys. Rev. Lett. 102, 107602 (2009).

[47] A. Janotti, L. Bjaalie, L. Gordon, C.G. Van de Walle, Phys. Rev. B, 86, 241108 (2012).

[48] N.C. Bristowe, P.B. Littlewood, E. Artacho, Phys. Rev. B, **83**, 205405 (2011).

[49] L. Yu and A. Zunger, Nat. Commun. 5, 5118 (2014).

[50] C. Cen, S. Thiel, G. Hammerl, C.W. Schneider, K.E. Andersen, C.S. Hellberg, J. Mannhart, J. Levy, Nat. Mater., 7, 298 (2008).

[51] R. Colby, L. Qiao, K. H. L. Zhang, V. Shutthanandan, J. Ciston, B. Kabius, and S. A. Chambers, Phys. Rev. B 88, 155325 (2013).

[52] J. M. D. Coey, M. Viret, S. von Molnár, *Adv. Phys.* **48**, 167 (1999).

[53] C. Weber, K. Haule, G. Kotliar, Nat. Phys., **6**, 574 (2010).

[54] P. Raychaudhuri, C. Mitra, P.D.A. Mann, S. Wirth, J. Appl. Phys. **93**, 8328 (2003).

[55] Q. Zhang, W. Zhang, Phys. Rev. B **68**, 134449 (2003).

[56] W. J. Lu, Y. P. Sun, B. C. Zhao, X. B. Zhu, W. H. Song, Phys. Rev. B **73**, 174425 (2006).

[57] S. Middey, M. Kareev, D. Meyers, X. Liu, Y. Cao, S. Tripathi, D. Yazici, M. B. Maple, P. J. Ryan, J. W. Freeland, J. Chakhalian, Appl. Phys. Lett. **104**, 202409 (2014).

[58] A. Gupta, T.R. McGuire, P.R. Duncombe, M. Rupp, J.Z. Sun, W.J. Gallagher, G. Xiao, Appl. Phys. Lett., **67**, 3494 (1995).

[59] J. Töpfer, J.B. Goodenough, J. Solid State Chem., **130**, 117 (1997).

[60] C. Aruta, M. Angeloni, G. Balestrino, N. G. Boggio, P. G. Medaglia, A. Tebano, B. Davidson, M. Baldini, D. Di Castro, P. Postorino, P. Dore, A. Sidorenko, G. Allodi, and R. De Renzi, J. Appl. Phys. 100, 023910 (2006).

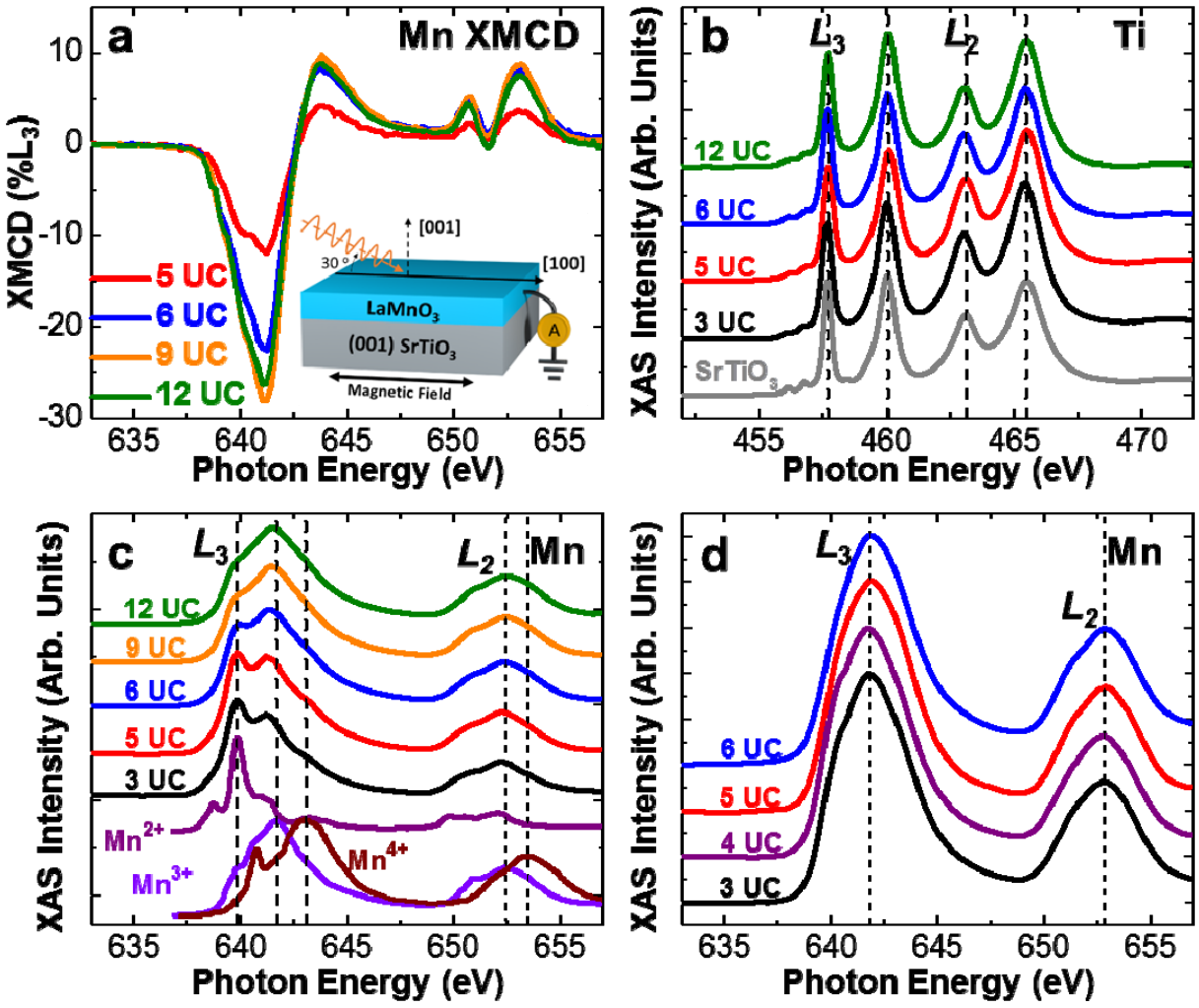

FIG. 1. (a) Mn XMCD spectra for various $LaMnO_3/SrTiO_3$ heterostructures. The inset shows a schematic of the experimental configurations for the X-ray spectroscopy studies. Thickness dependence of the XAS spectra of the $LaMnO_3/SrTiO_3$ heterostructures at the (b) Ti $L_{2,3}$, and (c) Mn $L_{2,3}$ edges with reference spectra for $SrTiO_3$, bulk $SrMnO_3$, $LaMnO_3$, and MnO for comparison. (d) XAS of Mn $L_{2,3}$ edges for various $LaMnO_3/NdGaO_3$ heterostructures where no reconstruction has occurred.

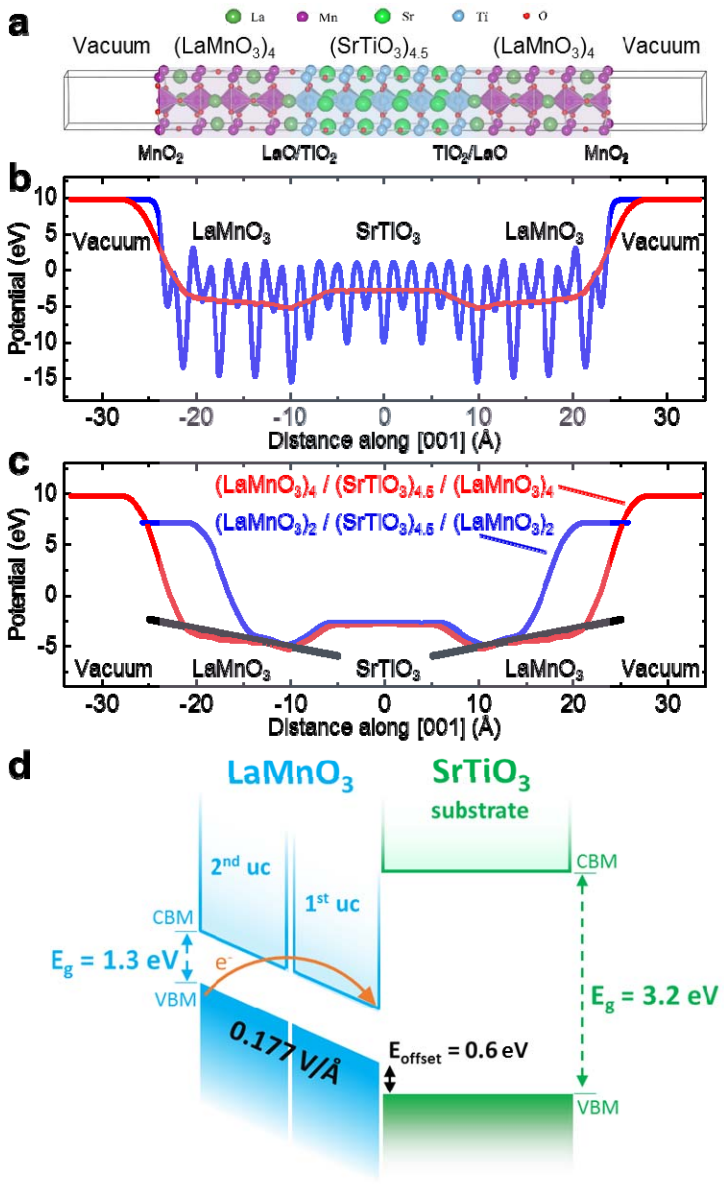

FIG. 2. (a) Schematic of the symmetric, vacuum-terminated $(LaMnO_3)_m/(SrTiO_3)_n/(LaMnO_3)_m$ slab with two identical *n*-type interfaces (here m = 4 and n = 4.5). (b) The in-plane average (oscillating blue line) and macroscopic average (red line) electrostatic potential across the $(LaMnO_3)_4/(SrTiO_3)_{4.5}/(LaMnO_3)_4$ simulation slab. (c) Comparison of the macroscopic average potential between the $(LaMnO_3)_4/(SrTiO_3)_{4.5}/(LaMnO_3)_4$ and $(LaMnO_3)_2/(SrTiO_3)_{4.5}/(LaMnO_3)_2$ heterostructures; the average intrinsic electric field is indicated by the black lines with a value of 0.177 V/Å. (d) Schematic band diagram of $LaMnO_3/SrTiO_3$ interface.

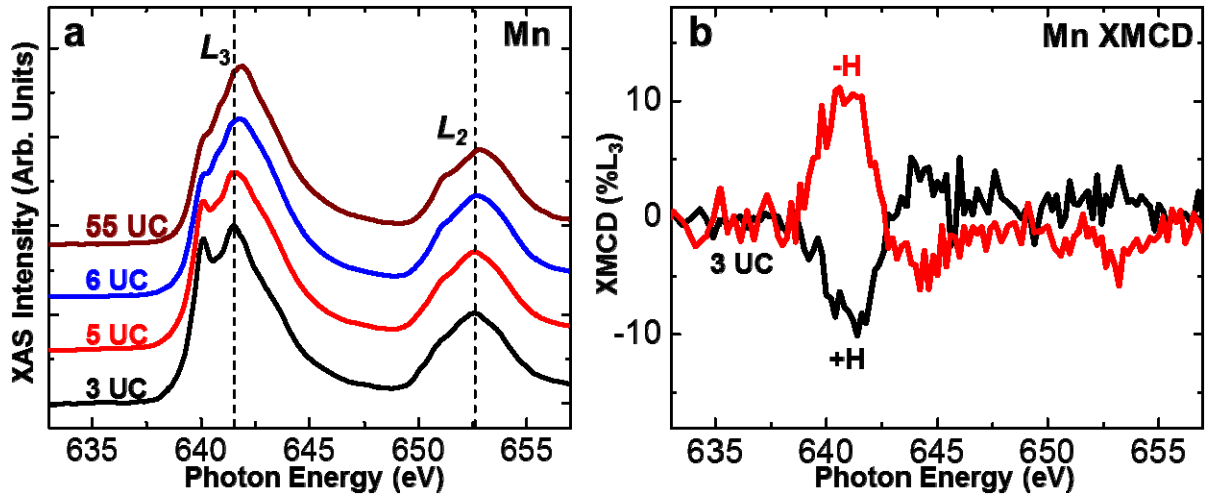

FIG. 3. (a) Mn $L_{2,3}$ XAS spectra of the $La_{0.95}MnO_3/SrTiO_3$ heterostructures. (b) Mn XMCD spectra for the 3 UC $La_{0.95}MnO_3/SrTiO_3$ heterostructure. The XMCD features reverse in sign when the magnetic field is reversed, confirming the reliability of the observation.